Research Article | Vol. 26, No. 23 | 12 Nov 2018 | OPTICS EXPRESS 30000
Optics EXPRESS

Integrated optical frequency domain reflectometry device for characterization of complex integrated devices

LUIS A. BRU,[1] DANIEL PASTOR,[1,*] AND PASCUAL MUÑOZ[1,2]

[1] *Photonics Research Labs, Universitat Politècnica de València, c/ Camino de Vera s/n, 46021 Valencia, Spain*
[2] *VLC Photonics S.L., c/ Camino de Vera s/n, 46021 Valencia, Spain*
[*] *dpastor@dcom.upv.es*

Abstract: Because of the demand for advanced measurement systems in the field of modern photonic integrated circuits, optical frequency domain reflectometry (OFDR) is a robust technique for characterizing design-to-fabrication deviations. In this paper we report an OFDR device where the interferometric part is monolithically integrated along with the device under test. We discuss the advantages in terms of compactness and performance, and the importance of the incorporated dispersion de-embedding mechanism. Experimental validation is carried out by interrogating an arrayed waveguide grating on a silicon nitride platform. The results establish the proposed device as a first step in the quest for a universal test structure for integrated devices.

1. Introduction

The growing complexity in modern photonic integrated circuits (PICs) makes advanced measurement systems necessary to provide a more complete optical characterization of them. The actual performance of the integrated devices composing a PIC is affected by errors in the fabrication process and therefore deviates from the numerical simulations. Spurious reflections, phase errors, etc. as well as unpredicted couplings between them accumulate as the PIC scales up, increasingly complicating the task of identifying them just from conventional spectral measurements, where a broadband source and an optical spectrum analyzer (OSA) are typically employed (or any equivalent setup). The lack of optical phase information resolution hinders this task even considering single complex devices like arrayed waveguide gratings (AWG).

A superior measurement system able to resolve optical amplitude and phase response is required and optical frequency domain reflectometry (OFDR) [1–4] has already been proposed by the scientific community to address characterization in the context of integrated devices [2, 5–10]. Along with optical time domain reflectometry (OTDR) [11] and low coherence frequency domain reflectometry (OLCR) [12], OFDR is one of the main interferometric techniques which have tradeoffs in terms of sensitivity, accuracy, speed, length range and resolution. OFDR is appealing due to its simpler setup implementation (fully passive with no mobile parts) and still high sensitivity, length range and spatial resolution [3].

The passive nature of the interferometric part of the OFDR setup motivates the integration of it, for the sake of compactness and stability that integrated waveguides (IW) can uniquely provide. In this direction, the authors in existing literature [5–7] took advantage of high reflectivity of the chip facets to create Fabry-Perot type interferometers generating the interferograms. In [6, 7], by de-embedding waveguide dispersion, a method to estimate the group refractive index and localize on-chip reflective events is proposed. A homodyne detection scheme is not explicitly used and it is a tunable laser source (TLS) step-by-step scanning which provides the necessary wavelength (or frequency) referencing. In our approach we intendedly integrate the whole interferometric setup, including triggering (TRIG) and device under test (DUT) interferometers, both of them

#340361 https://doi.org/10.1364/OE.26.030000
Journal © 2018 Received 25 Jul 2018; revised 7 Sep 2018; accepted 10 Sep 2018; published 31 Oct 2018

Optics EXPRESS

being Mach-Zehnder interferometers (MZI). As we shall discuss in the following section, this integrated version (IOFDR) could be considered a more general approach as it potentially applies to a broader range of cases and additionally provides an alternative way to deal with dispersion, a crucial parameter as it ultimately limits the spatial resolution of the system.

The paper is structured as follows: first we overview the fundamentals of OFDR technique and discuss the details of the integrated version, paying special attention to the dispersion impact on them in section 2. In section 3 we present our IOFDR implementation with an AWG as the DUT, where the performed measurements provide experimental validation of the proposed device, also contrasting with external OFDR setup measurements. Finally, we present our conclusions and discussion on further directions in section 4.

2. Integrating OFDR

The OFDR technique is a measurement system resolving optical amplitude and phase response of a DUT in both frequency and time domains, based on sweep-wavelength homodyne interferometric detection. As shown in Fig. 1(a), after TLS scanning the upper interferometer (DUT-MZI) generates the DUT beating signal, which is photodetected and resampled by points provided by the triggering interferometer (TRIG-MZI) detected interferogram, so it is self-referenced against TLS continuous sweep nonlinearities. Polarization controllers (PC) are commonly employed in an external fiber-based OFDR setup to both select polarization state of incidental light on the DUT (PC1) and to avoid polarization misalignment when beating the signals coming from the arms of the interferometers (PC2 and PC3). By applying inverse fast Fourier transform (IFFT) algorithm to the DUT interferogram, the corresponding time domain response (amplitude and phase) is obtained, where events are visualized so they can be sliced, bandpass filtered (in a temporal sense) and transformed by FFT back to the frequency domain, allowing spectral reconstruction of selected events. Path length differences (PLD) of both MZIs (ΔL and $\Delta L'$) are related to their corresponding interferograms free spectral range (FSR) as FSR $\simeq \lambda^2/(n_g \Delta L)$ so they must be carefully chosen for a correct resampling: supposing a given ΔL, Nyquist criterion establishes $\Delta L' \geq 2\Delta L$ to avoid aliasing. Therefore, since $\Delta L' \simeq 4\Delta L$ 'safely' places the DUT time domain response in the center of the time domain semi-window, whose width $\Delta L'/2$ has to be ensured to be wide enough to hold the entire DUT spatial width (Δz_{DUT}), it should be met the condition $\Delta L \geq \Delta z_{\mathrm{DUT}}/2$.

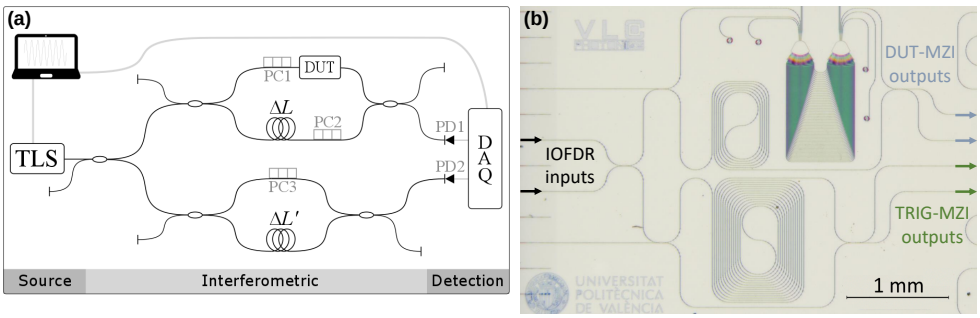

Fig. 1. (a) Schematic picture of a conventional (fiber-based) OFDR measurement setup in transmission mode. (b) Microscope picture of the IOFDR chip: both MZIs with their corresponding delay lines (spirals) are designed together with the AWG as the chosen DUT.

There are arguments enough to consider the integration of the interferometric part of an OFDR, employing IWs to replace the optical fibers. The most obvious is the miniaturization, not just as a matter of size as they allow to tailor much shorter PLDs for the interferometers, thus allowing to accurately design a narrower time window sufficient to hold the whole integrated DUT time

domain response. Thanks to this measure, the subsequent larger FSRs make the interferograms to be resolved more reliably by the photodetection and acquisition parts, even allowing the possibility of employing a lower performance detection part. Regarding the IWs as the propagating media, they are less sensitive to external conditions than optical fibers, improving the reliability and repeatibility of the measurements. On the other hand, the fact IWs present higher losses is not necessarily critical: the fringes visibility maximizes the closer the interference arms optical powers are. For the DUT-MZI in the integrated approach, light follows two different paths which accumulate similar losses (associated to the chip coupling and propagation), something that does not happen with an external OFDR where the reference arm power should be attenuated to meet the condition. Additionally, the IWs shorter lengths help to restrict their high accumulated propagation losses, a valid argument for the accumulated dispersion too. However, the presence of dispersion, typically high in IWs, is a particularly sensitive issue in an OFDR technique as it ultimately limits the spatial resolution of the system (determined by the sweep span [2]), and especially critical when dealing with the small feature sizes involved in the integrated devices. Indeed, a solution to de-embed the IW dispersion turns necessary to properly resolve the time domain response of the DUT as we show in the next subsection 2.1, where we shall discuss in detail how the proposed IOFDR deals with this issue.

To end this general discussion, we consider two points at the layout level: on the one hand, due to technological reasons in some cases unwanted contributions may be expected coming from cavities generated by on-chip reflections on chip facets, stitching transitions, etc. MZIs path lengths can be engineered to avoid them to couple to the DUT response, even making a wider time domain window to pre-allocate them, so that IOFDR technique is versatile against these possible contributions. On the other hand, we remark the versatility provided by the employment of MZIs, in the sense that they are potentially adaptable to transmission or reflection interrogation of the DUT and allow any coupling strategy to chip (either butt or vertical coupling). They also minimize, in comparison to other interferometers, the presence of higher-order beatings feedback.

2.1. Dispersion de-embedding mechanism

The presence of chromatic dispersion [2] in DUT and MZI waveguides impacts OFDR in two ways. To argument this, let us consider a general case where DUT and MZI waveguides have different arbitrary propagation constants β and β', respectively. We first consider the DUT-MZI where we have a DUT of length L whose transfer function is given by $H(\omega) = |H(\omega)| \exp(i\phi(\omega)) \exp(i\beta L)$ (with the propagation part explicitly separated). Assuming no losses, the oscillatory part of the resulting DUT-MZI interferogram can be described by:

$$I = 2\,|H(\omega)| \cos\left(\beta'(\omega)\,(\Delta L + L) - \beta(\omega)L - \phi(\omega)\right). \tag{1}$$

Considering the TRIG-MZI, the oscillatory part of the resulting interferogram I' provides the set of sampling points β'_μ as the rising roots of the sinusoid,

$$I' \propto \cos\left(\beta' \Delta L'\right) \rightarrow \beta'_\mu = \frac{\frac{3\pi}{2} + 2\pi\mu}{\Delta L'}, \text{ where } \mu \in \mathbb{Z}. \tag{2}$$

Following the OFDR process, the points β'_μ in Eq. (2) resample the DUT-MZI interferogram in Eq. (1) in order to remove nonlinearities coming from the TLS sweep (not included in this model) and provide a linearization in ω, a required condition to properly apply the FFT algorithm. In a conventional OFDR setup, where optical fibers are the common waveguides employed for the MZIs, it can be assumed $\beta'(\omega) \propto \omega$ in the working bandwidth, ensuring the linearization in ω. In this case, the presence of DUT dispersion given by β manifests as a chirp in the DUT-MZI interferogram entailing a broadening of the time domain events that, in turn, limits the ideal spatial resolution in OFDR $\delta z_{\text{id}} = \lambda^2/\left(n_g \Delta\lambda\right)$, determined by the sweep span $\Delta\lambda$ and being n_g

the average group index. A technique to de-embed dispersion would be required, being the common way to assume a second-order model to fit the interferogram so that once parameters are deduced, interferogram is inversely chirped (e.g. by a nonlinear resampling) [2, 6].

However, in light of Eq. (2), when the condition $\beta'(\omega) \propto \omega$ cannot be met (as it is the case when we consider IWs), it can be only ensured a linearization in β' with a step of $\delta\beta' = 2\pi/\Delta L'$. In this way, for arbitrary non-trivial β' we have a complicated scenario where the resampling is made, in general, nonlinearly in ω of a DUT response whose waveguides have a different propagation constant. Nonetheless, it is reasonable to make an important assumption in the case of IOFDR: the IWs conforming the DUT and the MZIs can be considered the same in terms of propagation conditions, provided that the DUT possible different sections are short and/or not too different. This consideration can be adopted in the analysis by computing $\beta = \beta'$, so that by introducing (2) in (1) we obtain the resampled DUT interferogram as:

$$I_\mu = 2\left|H\left(\beta_\mu\right)\right| \cos\left(\left(\frac{3\pi}{2} + 2\pi\mu\right)\frac{\Delta L}{\Delta L'} - \phi\left(\beta_\mu\right)\right). \tag{3}$$

In Eq. (3) we have, on the one hand, the amplitude of the DUT modulating a cosine. Within, depending on the PLDs ratio $\Delta L/\Delta L'$ there is a constant phase, and a linear term on μ that basically traces the cosine function. Last, and most importantly, there is the optical phase response of the DUT sampled linearly in β_μ (as given by Eq. (2)) as the only arbitrarily varying phase term. Any nonlinear β dependence is automatically cancelled, having a very special case where *IOFDR inherently provides a compensated version of the DUT response regardless of the degree and order of present dispersion of the waveguides.* This is a remarkable characteristic as it permits to tighten the actual spatial resolution of the system to the ideal one, especially important when considering integrated DUTs where feature sizes are particularly small and dispersion is often some magnitude orders above than in optical fibers. From another point of view, what we formally obtain after applying IFFT with this particular linearization in β, which is ultimately responsible of the dispersion de-embedding mechanism, is the spatial domain response of the DUT, a version of the impulsive domain free from time-related effects like temporal broadening.

To illustrate this, in Fig. 2(a) is shown a simple numerical simulation of an AWG with a FSR of 32 nm and 41 waveguides in the array: the expected train of pulses separated 0.24 ps are completely superimposed and indistinguishable when measuring with MZI waveguides being fiber (i.e. $D_{\text{fib}} \simeq 18$ ps/(nm km), lengths in the order of meters, PLDs in tens of cm) the AWG, whose IWs have a measured dispersion of $D_{\text{iw}} = -1430$ ps/(nm km) [10]. In Fig. 2(b), the same

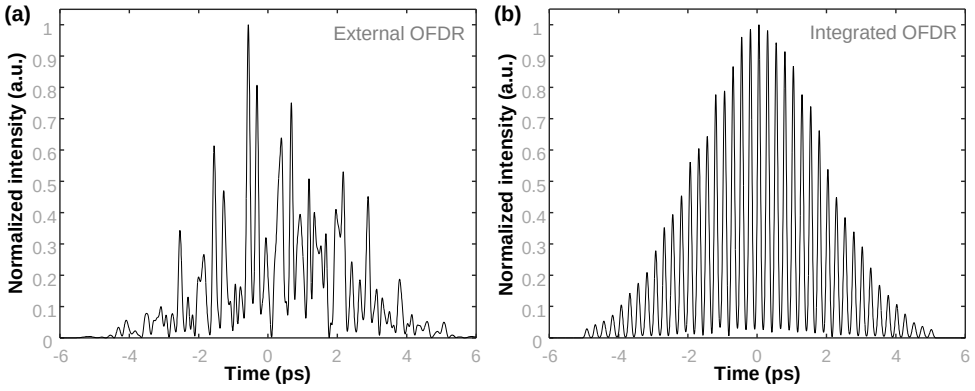

Fig. 2. Time domain response of a 41-waveguide AWG simulated to be measured with an external OFDR (a), and with an IOFDR system (b).

AWG in the IOFDR approach, where the lengths are similar to the designed ones (few cm, see

Optics EXPRESS

next section), shows an almost perfect comb of AWG contributions, being the slight distortion of the gaussian envelope the only visible effect due to the weak interaction between the adjacent contributions.

2.2. Propagation properties

The dispersion de-embedding mechanism is a strong point of the IOFDR approach: it automatically provides a perfect compensation of any order of dispersion present in the IWs. However, any possibility of directly quantifying it (e.g. by fitting to a theoretical model as in Refs. [2, 6]) is rejected, since the corresponding phase contributions overlap the TLS sweep nonlinearities in the interferograms, getting cancelled after resampling process. Group index n_g can be though derived directly from the IOFDR measurement: from Eq. (2), the step $\delta\beta = 2\pi/\Delta L'$ determines the β span as $\Delta\beta = N\delta\beta$, where N is the number of oscillations in the swept band. On the other hand, assuming a second-order dispersive medium, it is straightforward to relate to wavelength as $\Delta\beta = 2\pi n_g \frac{\Delta\lambda}{\lambda_1\lambda_2}$ (it can be shown that this expression for $\Delta\beta$ is only affected by odd-order terms of the $\beta = \beta(\omega)$ series). By equating both expressions, n_g can be solved as

$$n_g = \frac{\lambda_1\lambda_2}{\Delta\lambda\Delta L'}N, \tag{4}$$

in such a way that n_g can be estimated by relying on sweep wavelength boundaries, the designed $\Delta L'$ for the TRIG-MZI, and the observed number of oscillations N (this derivation is equivalent to the employed in [13]).

In order to estimate higher-order propagation parameters a reliable reference to actual frequency would be required to isolate dispersion effects in the interferogram. Therefore, in case of being interested on calculating dispersion parameters in IOFDR, it should be used the approach followed in [6]: a TLS step-by-step scanning avoiding nonlinearities, so the contained phases in the interferogram would come only from the IW dispersion, then computing a fitting to a theoretical model.

3. Experiment

In this section we report the experimental validation of the proposed IOFDR. The device chip was fabricated on the CNM-VLC silicon nitride platform, where a Si_3N_4 guiding film height of 300 nm is fabricated by low pressure chemical vapor deposition (LPCVD) over a 2.5 μm SiO_2 buffer platform, and covered by a deposited 2.0 μm SiO_2 cladding by plasma-enhanced chemical vapor deposition (PECVD) [10, 14]. Deeply etched rectangular waveguides of 1 μm width designed for single-mode operation at $\lambda = 1550$ nm are employed for the routing.

A picture of the fabricated device is shown in Fig. 1(b). The device is fed via one of the two central inputs at left facet, then reaching a first power splitter implemented by 50:50 multimode interferometers (MMI couplers). Next, the signal is routed to the MZIs, where DUT and TRIG interferograms are correspondingly generated. To engineer the spatial domain parameters as described in previous section, a spiral of 1.30 cm implements a PLD for the DUT-MZI of $\Delta L = 0.98$ cm to account for DUT length (approximately 0.30 cm). For the TRIG-MZI, a spiral of 4 cm is chosen to have $\Delta L' = 3.69$ cm. The beating signals are simultaneously collected at two of the four available outputs, to be photodetected. The DUT is a 5×5 channel AWG designed with 59 waveguides in the array and a FSR of 32 nm (4 THz).

3.1. Measurements and performance

For the measurements, a TLS (Yenista TUNICS T100R) provides the swept signal which is end facet coupled to the chip, making use of a polarization controller plus microscope objective and a linear polarizer to ensure fundamental TE mode excitation. After travelling through the chip

Optics EXPRESS

circuitry, the light is collected simultaneously at both the TRIG and the DUT outputs by means of a lensed fiber array. Both signals are photodetected by InGaAs photodiodes (Thorlabs FGA01FC) and the resulting electrical signal is converted to digital data by means of data acquisition card (DAQ, National Instruments USB-6259), thus prepared to be post-processed. The TLS scan is centered at 1550 nm, with span $\Delta\lambda = 80$ nm. The recorded interferograms are shown in Fig. 3. The chosen scan speed $v = 20$ nm/s and moderately low acquisition rate of 10 kS/s per channel allow a step of 2 pm/S, more than enough to properly resolve the corresponding DUT and TRIG interferograms whose FSRs are 130 pm and 30 pm, respectively. As designed, the TRIG-MZI generates interference fringes (green) with a FSR close to a fourth the corresponding ones to the DUT-MZI. In the interferograms, the extinction ratio (ER) decreases for increasing wavelengths, due to a change of the MMIs splitting ratio. The wavelength-dependent DC level is removed by post-processing: a moving mean algorithm is applied to the raw measured interferograms (shown in the left inset of Fig. 3) in order to estimate a local mean vector (represented by the black thick curves), that it is then subtracted from the interferograms (right inset). Next, by

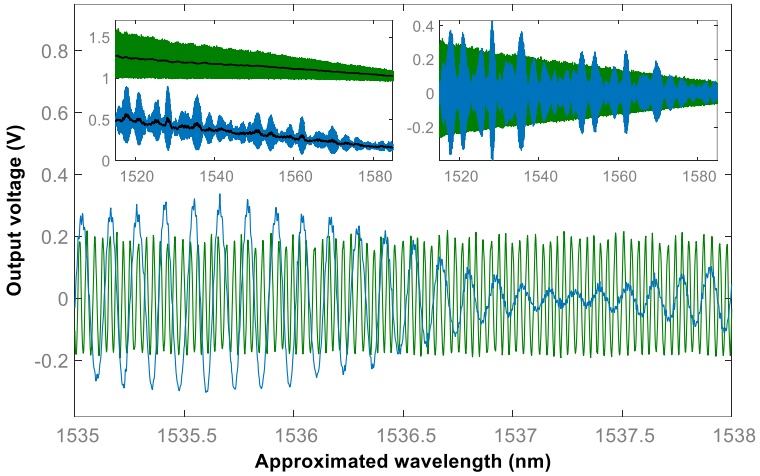

Fig. 3. Interference fringes corresponding to the TRIG-MZI (green curve) and to the DUT-MZI (blue curve) after removing DC level. In the right inset, the same plots in a broader wavelength range. In the left inset, the raw measured interferograms are shown.

applying the IFFT to the triggered DUT interferogram (after using a gaussian window function to minimize the edge effects, reducing them to about 3 dB), the spatial domain response is obtained, as previously described. From the number of sampling points in the working wavelength span, using formula (4) we deduced $n_{g,\mathrm{exp}} = 1.894 \pm 0.001$, a value very close to the simulated group index for fundamental TE mode $n_g = 1.932$. In Fig. 4(a) (black solid curve) the AWG spatial domain response is shown: the train of waveguide pulses, whose measured average separation is 37.3 ± 0.1 μm (compatible with the 38.8 μm in the design to achieve the targeted FSR) is perfectly distinguishable with a high visibility and with the characteristic slab coupler far field gaussian envelope [15, 16]. The deviations from the gaussian envelope are likely due to a combination of actual events such as waveguide imperfections and polarization fadings, as well as the previously illustrated measurement induced pulse overlap (as we observed in the simulations in Fig. 2(b)).

The experimental spatial resolution of the system can be estimated by computing the full width at half maximum (FWHM) of fitted gaussian functions to the AWG peaks of a selected set, in particular the 34 central ones enclosed by the grey dashed vertical lines in Fig. 4(a): the calculated average spatial resolution is $\delta z_{\mathrm{exp}} = 18.5 \pm 1.7$ μm, whose associated error contains the ideal value which we calculated to be $\delta z_{\mathrm{id}} = 17.4$ μm, corresponding to the analyzed (slightly

Optics EXPRESS

reduced) $\Delta\lambda$ and derived n_g. This constitutes a robust proof of the dispersion de-embedding mechanism described in subsection 2.1. In Fig. 4(b), the phase difference between consecutive

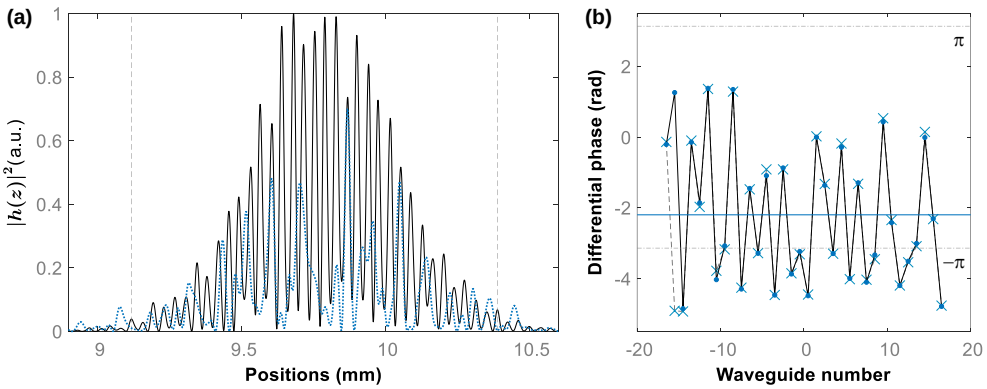

Fig. 4. (a) The spatial domain response of the AWG from IOFDR (black solid curve) and external OFDR (blue dotted curve) measurements. The phase difference between the consecutive contributions enclosed by the vertical lines, resolved by IOFDR, is shown in (b).

AWG arrayed waveguides contributions (from the selected set, taken at the peaks) is shown, where two traces corresponding to two different measurements have been included (represented by points and crosses) to verify the acceptable consistency of the technique to resolve the optical phase. By design, the phase difference is constant since AWG is designed with a constant length difference between consecutive waveguides, as well as with perfect focusing from (to) the AWG input (output) waveguides. For this particular and specially selected DUT, the measured phase errors [15] are sign of an AWG with degraded response [16], as shown in Fig. 5 on the next subsection. For completeness, the observed average phase difference (represented by the blue straight line) is related to the global phase given by (3) [17] combined to the real mean phase corresponding to the incremental length of the waveguides in the AWG.

3.2. Comparison with external fiber-based OFDR measurements

In this final part we show the external OFDR measurement of the AWG, in order to compare its performance with the IOFDR one. The use of an external OFDR setup to interrogate the DUT (the same combination of central input/output) is possible by accessing the device either through one of the main IOFDR inputs, or the free direct input to DUT-MZI above (since 2×2 MMI are used for the DUT-MZI). Similarly, the resulting signal is collected from the chip through one of the main outputs. The external MZIs are built with optical fibers and their corresponding PLDs are $\Delta L_{\text{ext}} = 13$ cm and $\Delta L'_{\text{ext}} = 83$ cm. This way, we are able to distinguish between the AWG and the reference arm contributions, in a time domain window whose width is an order of magnitude wider.

As we argued in section 2.1, the use of the same waveguides for both the DUT and the MZIs (i.e. the same propagation constant) automatically provides a dispersion-compensated version of DUT response. When using fibers, due to the huge offset between the propagation constants we can assume the fiber as a non-dispersive medium in a first approximation, so the IW dispersion is not compensated leading to a temporal broadening that corresponds to a spatial resolution of about 165 μm. In Fig. 4(a), the resulting spatial domain response for this case is shown in blue dotted curve where, in agreement with the simulations in Fig. 2, the interference between the broadened consecutive peaks prevents resolving the individual contributions.

The FFT can be applied to selected parts of the impulsive domain at will, so that the spectral response of that selection is recovered. To isolate the AWG contributions, we apply a rectangular

Optics EXPRESS

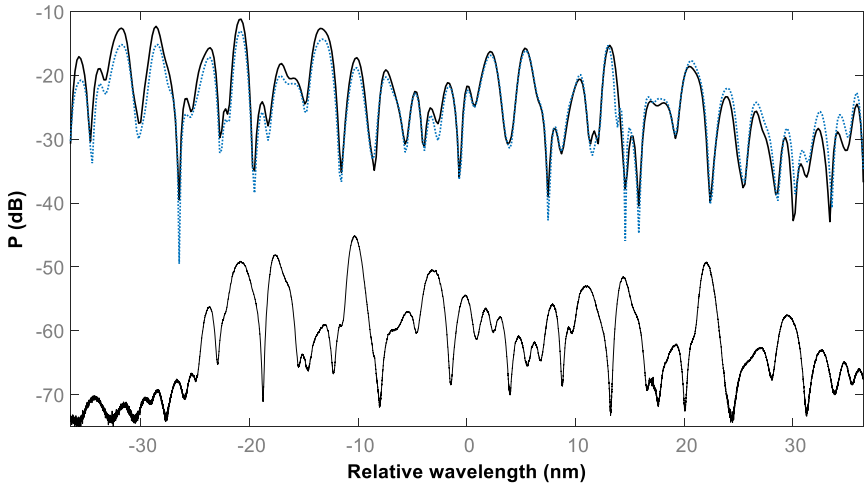

Fig. 5. Spectral reconstruction of the AWG spatial domain response from IOFDR (black thick curve) and external OFDR measurements (blue dotted curve). Below (black thin curve), spectral transmission measurement of a different combination of input-output AWG waveguides.

window function to the same section appearing in Fig. 4(a) (i.e. from 8.8 mm to 10.8 mm) since a smoothing to reduce edge effects is no needed. In Fig. 5 the spectral amplitude reconstruction of the AWG for the case of IOFDR measurement (black solid curve) and for the external OFDR (blue dotted curve) are shown. The almost perfect agreement between both traces demonstrates that even though the spatial response was not properly resolved by the external OFDR, the device still works the same way spectrally speaking. This is an important point: the IOFDR mechanism provides a mean to distinguish features temporally/spatially closer, but it actually does not change the performance of the device. In fact, as it can be seen in the Fig. 5, the defective performance of the AWG is there anyway. However, and remarkably, the IOFDR allowed us to locate the degradation source, and identify it as the strong phase variance between the waveguides in the array (Fig. 4(b)) thanks to the dispersion de-embedding intrinsic mechanism, otherwise not straightforward with conventional OFDR.

As a complementary evidence of the reliability of these spectral reconstructions, a measurement performed with classical equipment employing a broadband source (NP Photonics ASE-CL-17-S) and an OSA (Yokogawa AQ6370C) of a different combination of the AWG input-output waveguides is shown in Fig. 5. This AWG access is possible thanks to the inputs and outputs which keep outside the DUT-MZI in the design (see Fig. 1(b) the vertical waveguides exiting the AWG). We chose the immediately following input-output combination following the used central ones for the IOFDR measurement. In comparison to IOFDR and external OFDR reconstructions, the transmission spectrum (shifted about 10 nm due to the different combination choice) shows a very similar fashion confirming the defective performance of the AWG. A degradation of the chip facets nearby these input-output makes the acquired power to be very close to the noise floor as it can be noticed from the left part of the shown spectrum.

4. Conclusion

We have proposed the integration of an OFDR where the interferometric parts are co-integrated with the targeted DUT. Advantages in terms of compactness, performance reliability, as well as its potential applicability to a broad number of cases have been argued. The presence of a TRIG-MZI in the IOFDR device enables a powerful dispersion de-embedding mechanism, not

requiring further post-processing steps that need to assume an approximated model to account for any degree of dispersion. The IOFDR has been experimentally demonstrated by interrogating an AWG: we localized strong phase deviations in the waveguides of the array, perfectly resolved in its spatial response, and identified as the major cause of its degraded spectral performance. This identification was somehow not possible with the external OFDR setup. At the sight of these results, the IOFDR is a candidate for universal testing engine in integrated devices. Further work is underway in the direction of improving performance conceptually and by design, as well as to demonstrate the technique for other technologies and DUTs.

Funding

Spanish national projects, Ministerio de Economía y Competitividad (TEC2015-69787-REDT PIC4TB, TEC2016-80385-P SINXPECT, PTA2015-11309-I); Generalitat Valenciana (GVA PROMETEO 2017/103).

Acknowledgments

The authors acknowledge VLC Photonics S.L. and Instituto de Microelectrónica de Barcelona CNM-CSIC for the support in the design and subsequent fabrication of the measured chip samples on the cited CNM-VLC silicon nitride technology platform [14].

References

1. W. Eickhoff and R. Ulrich, “Optical frequency domain reflectometry in singlemode fiber,” Appl. Phys. Lett. **39**(9), 693–695 (1981).
2. U. Glombitza and E. Brinkmeyer, “Coherent frequency-domain reflectometry for characterization of single-mode integrated-optical waveguides,” IEEE J. Lightwave Technol. **11**(8), 1377–1384 (1993).
3. B. J. Soller, D. K. Gifford, M. S. Wolfe, and M. E. Froggatt, “High resolution optical frequency domain reflectometry for characterization of components and assemblies,” Opt. Express **13**(2), 666–674 (2005).
4. D. K. Gifford, B. J. Soller, M. S. Wolfe, and M. E. Froggatt, “Optical vector network analyzer for single-scan measurements of loss, group delay, and polarization mode dispersion,” Appl. Opt. **44**(34), 7282–7286 (2005).
5. F. Morichetti, “Roughness induced backscattering in optical silicon waveguides,” Phys. Rev. Lett. **104**, 033902 (2010).
6. D. Zhao, D. Pustakhod, K. Williams, and X. Leijtens,“High resolution optical frequency domain reflectometry for analyzing intra-chip reflections,” IEEE Photon. Technol. Lett. **29**(16), 1379–1382 (2017).
7. D. Zhao, D. Pustakhod, K. Williams and X. Leijtens,“High resolution optical frequency domain reflectometry for measurement of waveguide group refractive index,” in *P*roceedings of IEEE Photonics Conference (IEEE, 2017), pp. 537–538.
8. L. A. Bru, B. Gargallo, G. Micó, R. Baños, J. D. Doménech, A. M. Sánchez, R. Mas, E. Pardo, D. Pastor, and P. Muñoz, “Optical frequency domain reflectometry applied to photonic integrated circuits,” presented at European Conference on Integrated Optics (ECIO), paper o-08, Warsav, Poland, 18–20 May 2016.
9. L. A. Bru, Z. Ye, D. Pastor, and P. Muñoz, “Multi-parameter estimation of high-Q silicon rich nitride resonators using optical frequency domain reflectometry,” Proc. SPIE **10535**, 1053518 (2018).
10. P. Muñoz, G. Micó , L. A. Bru, D. Pastor, D. Pérez, J. D. Doménech, J. Fernández, R. Baños, B. Gargallo, R. Alemany, A. M. Sánchez, J. M. Cirera, R. Mas, and C. Domínguez, “Silicon nitride photonic integration platforms for visible, near-infrared and mid-infrared applications,” Sensors **17**(9), 2088 (2017).
11. M. K. Barnoski, M. D. Rourke, S. M. Jensen, and R. T. Melville, "Optical time domain reflectometer," Appl. Opt. **16**, 2375–2379 (1977).
12. R. C. Youngquist, S. Carr, and D. E. N. Davies, "Optical coherence-domain reflectometry: a new optical evaluation technique," Opt. Lett. **12**, 158–160 (1987).
13. Y. A. Vlasov, M. O’Boyle, H. F. Hamann and S. J. McNab, “Active control of slow light on a chip with photonic crystal waveguides,” Nature **438**(3), 65–69 (2005).
14. Silicon Nitride Photonic Integration Platform, http://www.imb-cnm.csic.es/index.php/en/clean-room/silicon-nitride-technology
15. P. Muñoz, D. Pastor, J. Capmany, and S. Sales, “Analytical and numerical analysis of phase and amplitude errors in the performance of arrayed waveguide gratings,” IEEE J. Sel. Top. Quantum Electron. **8**(6), 1130–1141 (2002).
16. P. Muñoz, D. Pastor, J. Capmany, D. Ortega, A. Pujol, and J. R. Bonar, "AWG Model Validation Through Measurement of Fabricated Devices," J. Lightwave Technol. **22**, 2763 (2004).
17. B. Robillart, C. Calo, A. Fall, F. Lamare, Y. Gottesman, and B-E Benkelfat, “Spectral and temporal phase measurement by Optical Frequency-Domain Reflectometry,” Proc. SPIE **8961**, 896134 (2014).